Chin. J. Astron. Astrophys. Vol. 6 (2006), No. 4, 477–488
(*http://www.chjaa.org*)

Chinese Journal of
Astronomy and
Astrophysics

The Relationship between Magnetic Gradient and Magnetic Shear in Five Super Active Regions Producing Great Flares *

Hai-Min Wang[1,2], Hui Song[2], Ju Jing[2], Vasyl Yurchyshyn[2], Yuan-Yong Deng[1], Hong-Qi Zhang[1], David Falconer[3] and Jing Li[4]

[1] National Astronomical Observatories, Chinese Academy of Sciences, Beijing 100012; *haimin@flare.njit.edu*
[2] Big Bear Solar Observatory, New Jersey Institute of Technology, Big Bear City, CA 92314, USA
[3] Marshall Space Flight Center, SD50, Huntsville, AL 35812, USA
[4] Institute for Astronomy, University of Hawaii, 2680 Woodlawn Drive, Honolulu, HI 96822, USA

Received 2006 January 17; accepted 2006 February 19

Abstract We study the magnetic structure of five well-known active regions that produced great flares (X5 or larger). The six flares under investigation are the X12 flare on 1991 June 9 in AR 6659, the X5.7 flare on 2000 July 14 in AR 9077, the X5.6 flare on 2001 April 6 in AR 9415, the X5.3 flare on 2001 August 25 in AR 9591, the X17 flare on 2003 October 28 and the X10 flare on 2003 October 29, both in AR 10486. The last five events had corresponding LASCO observations and were all associated with Halo CMEs. We analyzed vector magnetograms from Big Bear Solar Observatory, Huairou Solar Observing Station, Marshall Space Flight Center and Mees Solar Observatory. In particular, we studied the magnetic gradient derived from line-of-sight magnetograms and magnetic shear derived from vector magnetograms, and found an apparent correlation between these two parameters at a level of about 90%. We found that the magnetic gradient could be a better proxy than the shear for predicting where a major flare might occur: all six flares occurred in neutral lines with maximum gradient. The mean gradient of the flaring neutral lines ranges from 0.14 to 0.50 G km $^{-1}$, 2.3 to 8 times the average value for all the neutral lines in the active regions. If we use magnetic shear as the proxy, the flaring neutral line in at least one, possibly two, of the six events would be mis-identified.

Key words: Sun: activity — Sun: flares — Sun: magnetic fields — Sun: coronal mass ejections (CMEs)

1 INTRODUCTION

Solar flares and Coronal Mass Ejections (CMEs) are two related, and most important forms of explosive energy release from the sun. They can carry away an energy up to 10^{33} erg in a short period of time and can cause various effects in the heliosphere and the near earth environment. An important objective in solar physics research is to understand their physics and to predict their occurrence as early as possible. Among all the eruptive events, the most important ones are Halo-CMEs (earth directed CMEs) associated with X-class flares. Many of these events cause severe geo-magnetic effects and flood the near earth environment with large number of energetic particles.

* Supported by the National Natural Science Foundation of China.

It has long been noticed that non-potentiality of magnetic structure in the active region is vitally important in storing energy and triggering flares (Hagyard et al. 1984). The most notable indicator of non-potentiality is the δ sunspot, defined as umbrae of opposite magnetic polarity lying in a common penumbra. For over three decades, the morphological evolution of δ configurations and their strong connection to intensive flare activity have been widely studied (e.g., Tang 1983; Hagyard et al. 1984; Zirin 1987 ; Tanaka 1991). Using observations of 18 years at Big Bear Solar Observatory (BBSO), Zirin (1987) summarized the development of δ spots and classified them into three categories, concluding that δ groups are responsible for almost all the great flares.

Measurements of the global non-potentiality of an active region can be obtained from a vector magnetogram of the region regardless of the chirality of global magnetic shear or twist in the chromospheric or coronal images. For instance, such a measurement has been made in particular active regions to evaluate their potential of producing CMEs (Falconer 2001). Since the 1950's, the importance of magnetic gradient in producing solar flares has been recognized (see the review by Michard 1971). In particular, Severny (1960) gave a threshold value of 0.1 G km^{-1} as a preflare condition. Zhang (2001) found that the shear and gradient of the magnetic field are important in defining the non-potentiality of the active regions and reflect the strength of the electric current in the region. However, the analysis of vector magnetograms has experienced great difficulties even as new instruments are developed. The most notable difficulties are calibration, resolution of the 180 degree ambiguity and correction of the projection effect when the observed region is not close to the solar disk center.

From a sample of 17 vector magnetograms, Falconer, Moore & Gary (2003) showed that there is a viable proxy for non-potentiality that can be measured from line-of-sight magnetograms. This proxy is the strength of the magnetic gradient and is correlated with the CME productivity of the active region. Because the gradient can be measured from line-of-sight magnetograms obtained from conventional magnetographs, it may be a dependable substitute for magnetic shear for use in operational CME forecasting. Prasad (2000) used a similar parameter of magnetic gradient to characterize the stressed magnetic fields. However, so far there has been no study on a detailed comparison between the gradient and shear in active regions. This is the primary objective of this paper. Two questions will be addressed: (1) Are magnetic shear and gradient correlated? (2) Do flares tend to occur in the high gradient and/or high shear locations?

2 OBSERVATIONS

The primary data sources are from four well-known vector magnetograph systems:

(1) Digital Magnetograph (DMG) at BBSO. This is a filtergraph-based system. The bandpass of the birefringent filter is 1/4 Å, and centered at Ca I 6103 Å. The field-of-view of the instrument is $360'' \times 360''$ and the spatial resolution is $0.6''$ per pixel (Spirock 2005).
(2) Vector magnetograph at Huairou Solar Observing Station (HSOS) in China. The data were obtained by a filtergraph-based system that was developed by Ai (1987). It uses the Fe I 5324 Å. The bandpass of the birefringent filter is 1/8 Å. The field-of-view of the instrument is $360'' \times 240''$ and the spatial resolution is $0.6''$ per pixel.
(3) Vector magnetograph at Marshall Space Flight Center (MSFC). The magnetograph is a filter-based instrument employing a tunable Zeiss birefringent filter with a 1/8 Å bandpass and an electro-optical modulator to obtain integrated Stokes profiles in the Fe I 5250 Å absorption line. The field-of-view of the instrument is $420'' \times 300''$ and the spatial resolution is $1.28''$ per pixel.
(4) Imaging Vector Magnetograph at Mees Solar Observatory: It uses a tunable Fabry-Perot system with a pixel resolution of $1''$ FOV of $280'' \times 280''$ and polarization precision of 0.1% (Mickey et al. 1996). The data analysis procedures of IVM are more complicated than three other systems at BBSO, HSOS and MSFC. It requires full Stokes Inversion (LaBonte, Mickey & Leka 1999).

Table 1 compares the basic parameters of these vector magnetograph systems. According to the accuracy of each system, we estimated the probable errors when calculating the magnetic gradient and magnetic shear. The error in the azimuthal angle can only be estimated by inter-comparison of multiple instruments (Zhang et al. 2002; Wang et al. 1992). We believe that a 10-degree error is a reasonable value. We will see that most measurement errors on the various parameters are at least one order of magnitude smaller than the typical measured physical quantities themselves.

Table 1 Comparison of Magnetograph Systems

Magnetograph	BBSO	HSOS	MSFC	MSO
Wavelength	CaI 6103	FeI 5324	FeI 5250	FeI 6302
Bandpass (Å)	1/4	1/8	1/8	0.07
Pixel Resolution	$0.6''$	$0.6''$	$1.28''$	$1.0''$
Field of View	$360'' \times 360''$	$360'' \times 240''$	$420'' \times 300''$	$280'' \times 280''$
B Long. accuracy (G)	5	10	25	20
B Trans. accuracy (G)	100	200	75	200
Error in Gradient (G km^{-1})	0.012	0.024	0.026	0.030
Error in Shear (G×rad)	18	35	13	35

Table 2 Properties of Six Flares and the Active Regions

Date	91/06/09	00/07/14	01/04/06	01/08/25	03/10/28	03/10/29
Flare Time (UT)	0206	1023	1913	1631	1110	2047
Observatory	HSOS	HSOS	MSO	MSFC	BBSO	MSFC
NOAA Region	6659	9077	9415	9591	0486	0486
Location	N31E04	N22W07	S21E30	S17E34	S16E08	S15E08
Max Grad. AR NL (G km^{-1})	0.633	0.789	1.29	0.218	0.586	0.363
Max Grad. Flare NL	0.633	0.789	1.29	0.218	0.586	0.363
Mean Grad. AR NL	0.051	0.123	0.064	0.017	0.137	0.078
Mean Grad. Flare NL	0.389	0.383	0.503	0.136	0.314	0.207
Max Shear AR NL (G*rad.)	2478	1969	3125	2349	4040	4537
Max Shear Flare NL	2478	1969	3125	3521	4040	2039
Mean Shear AR NL	352	476	181	236	626	825
Mean Shear Flare NL	1544	1170	1397	757	2122	1287
Fitting Slope (radian*km)	3993	2444	2445	5549	4311	5769
C.C. AR NL	0.80	0.76	0.89	0.64	0.79	0.84
C.C. Flare NL	0.96	0.89	0.94	0.87	0.89	0.94
Shear as Predictor	Yes	Yes	Yes	No	Yes	No
Gradient as Predictor	Yes	Yes	Yes	Yes	Likely	Yes

The magnetograms presented in this paper were obtained between 1 and 6 hours before the flares, except that for the 2003 October 28 event, the first available magnetogram on that day was taken 4 hours after the flare. Because there is a sufficient gap between the time of observation and the time of the flare, possible contamination of magnetic signal by flare emissions is of no concern. On the other hand, many of our previous studies showed that the changes of magnetic structure of the AR are relatively subtle (less than 5% in 5 hours), so that the difference between the times of the flare and the magnetogram observation should not affect our basic conclusions. The first five rows of Table 2 list the basic information of the six flares studied in this paper. The flare morphological data are mainly given by TRACE white-light or 1600 Å images for the five post-2000 events, and by an Hβ image for the 1991 event. The other parameters will be explained in the next section.

The active regions were located not too far away from the disk center (maximum longitude is 34 degrees) when these large flares occurred. The measurement errors due to the projection effect of magnetic fields are comparable to the uncertainty levels presented in Table 1 (Li 2002). This will be discussed in more detail in Section 3.2. Furthermore, when the regions are within 45 degrees of the disk center, the 180-degree ambiguity can be resolved using the method developed by Moon et al. (2003). The basic assumption of this method is that the magnetic shear angle, which is defined as the difference between the azimuth of the observed and potential fields, approximately follows a normal distribution.

3 RESULTS

3.1 Bastille Day Flare on 2000 July 14

The Bastille Day flare on 2000 July 14 was well observed by many space and ground-based observatories. Its magnetic structure and flare emissions in many wavelengths have been studied by many authors (Liu &

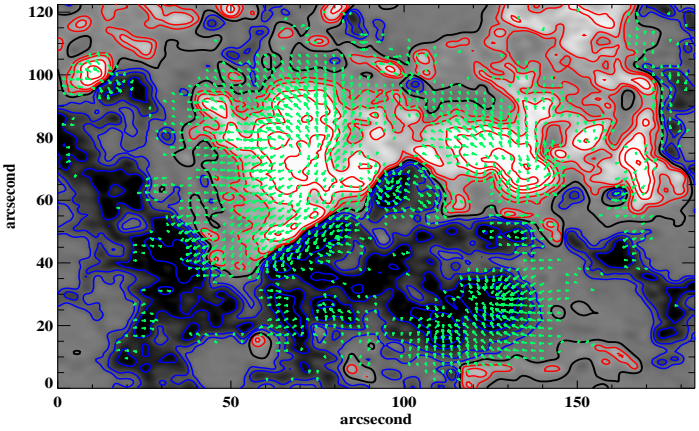

Fig. 1 HSOS Vector magnetogram obtained at 06 UT on 2000 July 14 for AR 9077. Gray scale represents line-of-sight magnetic field strength which is also plotted as contours (red: positive field, blue: negative). Contour levels are $\pm$200, 400, 800 and 1600 G. The green arrows indicate observed transverse fields. The longest arrow indicates a field strength of about 1800 G. Dark black lines are the magnetic neutral lines where the line-of-sight field is zero.

Zhang 2001; Yan et al. 2001; Deng et al. 2001; Masuda et al. 2001; Fletcher & Hudson 2001; Kosovichev & Zharkova 2001). Wang et al. (2005) found that this flare is one of many large flares that are associated with a very interesting evolutionary pattern: part of the outer δ spot structure decays rapidly after a major flare, while the central umbral and penumbral structures become darker. We use this event as an example to demonstrate our data analysis procedures and the significance of the results.

In Figure 1, we show a vector magnetogram taken by HSOS 6 hours before an observed flare. Based on this vector magnetogram, we generate three images: a magnetic gradient map, a shear map and a masking map marking the location of magnetic neutral lines. The magnetic neutral lines are defined by thick black lines in Figure 1. In this masking map, the intensity is 1.0, if a particular point is part of neutral lines, otherwise, the pixel value of this point is set to 0. The magnetic shear is defined as the product of observed transverse field strength and the shear angle. The shear angle is the angular separation between the directions of observed transverse fields and extrapolated potential fields. Wang et al. (1994) explained the reason of using this shear term instead of just the shear angle: (1) the stored magnetic energy through magnetic shear must be reflected by both field strength and shear angle; (2) the measurement of the direction of the transverse field sensitively depends on magnetic field strength: stronger fields would have lower measurement error. Consequently, the magnetic shear in the plot is in units of Gauss radian. The magnetic gradient map is constructed based on line-of-sight magnetogram only. As magnetic gradient is proportional to the derivative of the measured fields, we need to be aware that the random noise might have been enhanced significantly in the gradient maps. We use the software developed by Gallagher that is being used in the Active Region Monitor (Gallagher, Moon & Wang 2003), based on a finite difference scheme in which the derivatives at the borders are taken care of. To make the results more uniform and subject less to the variation in the seeing, we smooth the magnetograms with a kernel of $3''$ before doing the gradient calculation. As a consequence, the real gradient might be larger than the values presented in the paper. The errors of the gradient calculation are shown in Table 1.

Next, we multiply the shear image by the mask image to generate an image of shear in the neutral lines only. Similarly, we multiply the gradient image by the mask image to generate an image of gradient in the neutral lines only. Figure 2 shows the scatter plot of magnetic shear versus magnetic gradient for all the points along all the magnetic neutral lines in the active region. The plus signs represent points in the section of flaring neutral line. Apparently, these points (plus signs) have both higher magnetic shear and gradient than other points (dots) in the active region. More quantitative comparison is presented in Table 2 and will be discussed in Section 3.2. Furthermore, it is evident that there is a positive correlation between

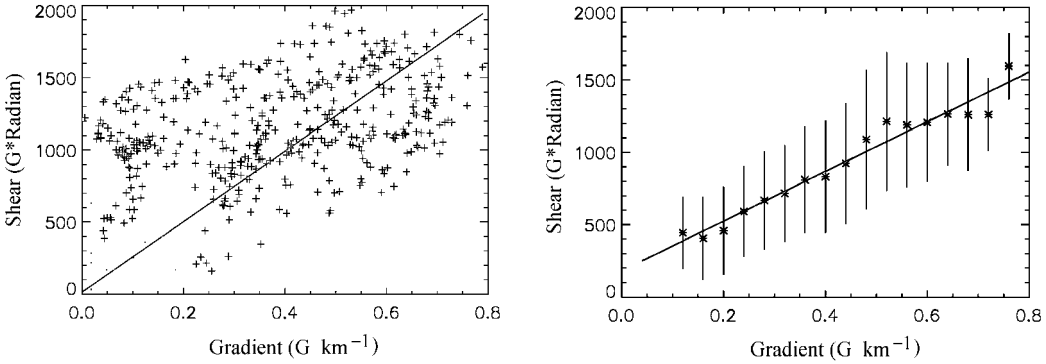

Fig. 2 Left: Scatter plot of magnetic shear vs. magnetic gradient in all the points along all the neutral lines identified for the active region 9077 on 2000 July 14. Plus signs are the points along the flare neutral line. The solid straight line is a linear fit of all the data points. Right: Plot of averaged magnetic shear vs. magnetic gradient with a linear fit. Vertical bars present standard deviation of shear in each bin.

the magnetic gradient and the magnetic shear. Although a large scatter is present in the plot, the linear relationship between the two parameters (gradient and shear) is still obvious. The correlation coefficient (C.C.) is 76% if using all the points in the active region. However, if only the points at the flaring neutral line are used, the C.C. increases to 89%. Comparable C.C. values between 87% and 96% are found for the other events. The fitted slope is 3993 km*radian, which is in between 2444 and 5769 km*radian for all the other events. The figure also includes an average plot with a bin size of 0.04 G km $^{-1}$ to show up the trend better. The fitted line is flatter due to the fact that there are fewer points in the high shear/gradient area.

In Figure 3 we show maps of magnetic gradient, gradient at the neutral lines, magnetic shear and shear at the neutral lines. In addition, the flare emissions are shown by a TRACE WL image. Obviously, the flare neutral line has both strong magnetic gradient and magnetic shear. Either the magnetic gradient or the magnetic shear can be used to identify correctly the flaring neutral line.

Table 3 Effects of Projection Correction for the 2001 April 6 Flare

Parameters	Before Correction	After Correction
Max Grad. AR NL (G km^{-1})	1.29	1.27
Max Grad. Flare NL	1.29	1.27
Mean Grad. AR NL	0.064	0.061
Mean Grad. Flare NL	0.503	0.453
Max Shear AR NL (G*rad.)	3125	2453
Max Shear Flare NL	3125	2453
Mean Shear AR NL	181	167
Mean Shear Flare NL	1396	1316
C.C. AR NL	0.89	0.75
C.C. Flare NL	0.94	0.80
Shear as Predictor	Yes	Yes
Gradient as Predictor	Yes	Yes

3.2 Summary of the Other Five Events

We present a comparison of shear and gradient maps in Figures 4–8 for the other five events. The parameters concerning the shears and gradients are listed in Table 2. There are four derived parameters for each: maximum value along all the neutral lines in the active regions, maximum value along the flare neutral line, mean value along all the neutral lines and mean value along the flare neutral line. The flare neutral line is defined by the extent of flare ribbons at the emission maximum. From this table, it is obvious that for all the six events, the maximum gradient along the flare neutral lines is the maximum gradient for the entire active

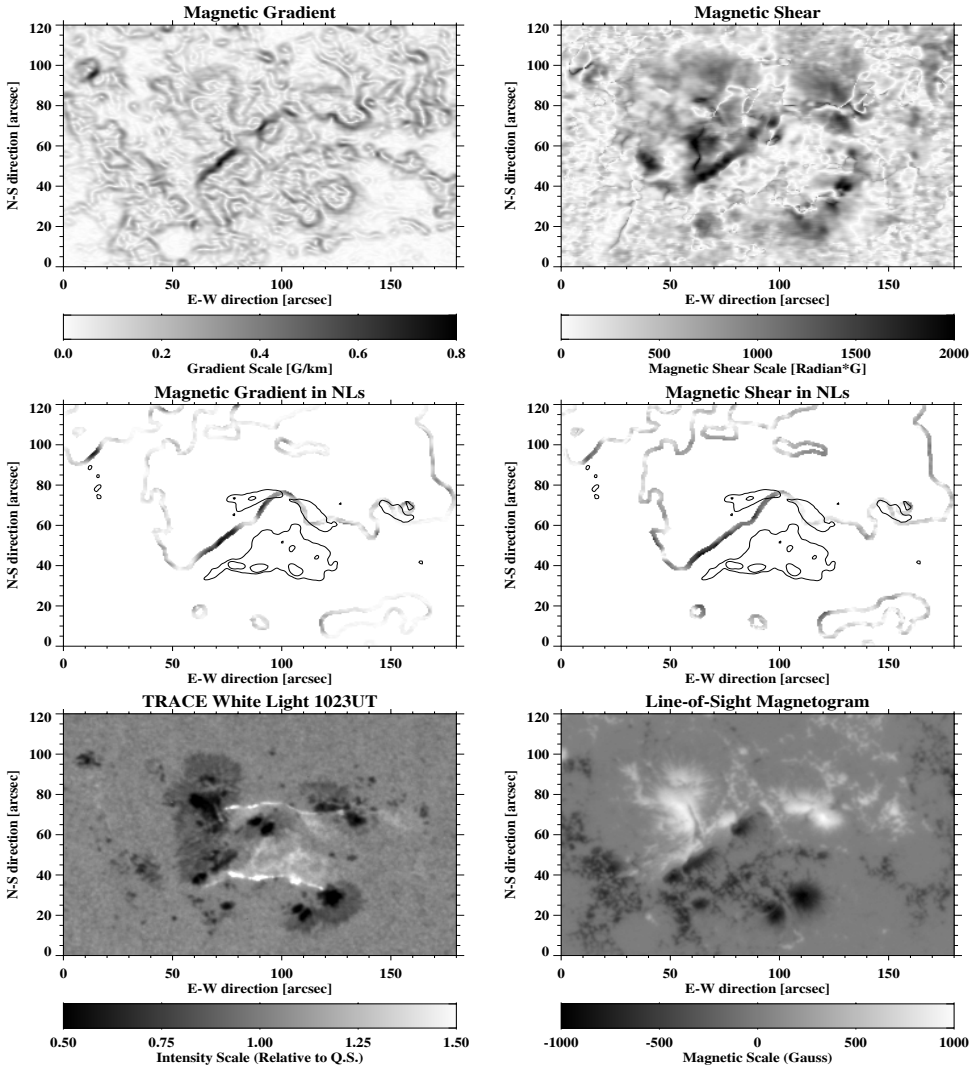

Fig. 3 Top left: magnetic gradient map of 2000 July 14; Top right: magnetic shear map; Middle left: magnetic gradient in neutral lines; Middle right: magnetic shear in neutral lines; Flare emissions are also plotted as contours (thin solid lines) in the two middle panels. In this figure and other similar figures below, the shear and gradient are presented in negative images, i.e., darker points show stronger shear or gradient. Bottom left: TRACE WL image to indicate the flare emissions; Bottom right: line-of-sight magnetogram.

region; the ratio of mean gradient along the flare neutral line to that of entire active region is between 2.3 and 8.0. The two lowest values of this ratio belong to the 2003 October 28 and 29 events. It is not difficult to explain such a low ratio for these two events: two flares occurred in the same active region but at two different locations. Both locations have high gradient (and shear as well). Therefore, either one of these two flare neutral lines can not be uniquely dominant in having high mean gradient (or shear). Based on this analysis, we can confidently conclude that the high magnetic gradient is a good indicator of the location of these large flares. If we do a similar analysis for the magnetic shear, then, maximum magnetic shear in active regions is not located at the flare neutral lines for the 2001 August 25 and 2003 October 29 events. In

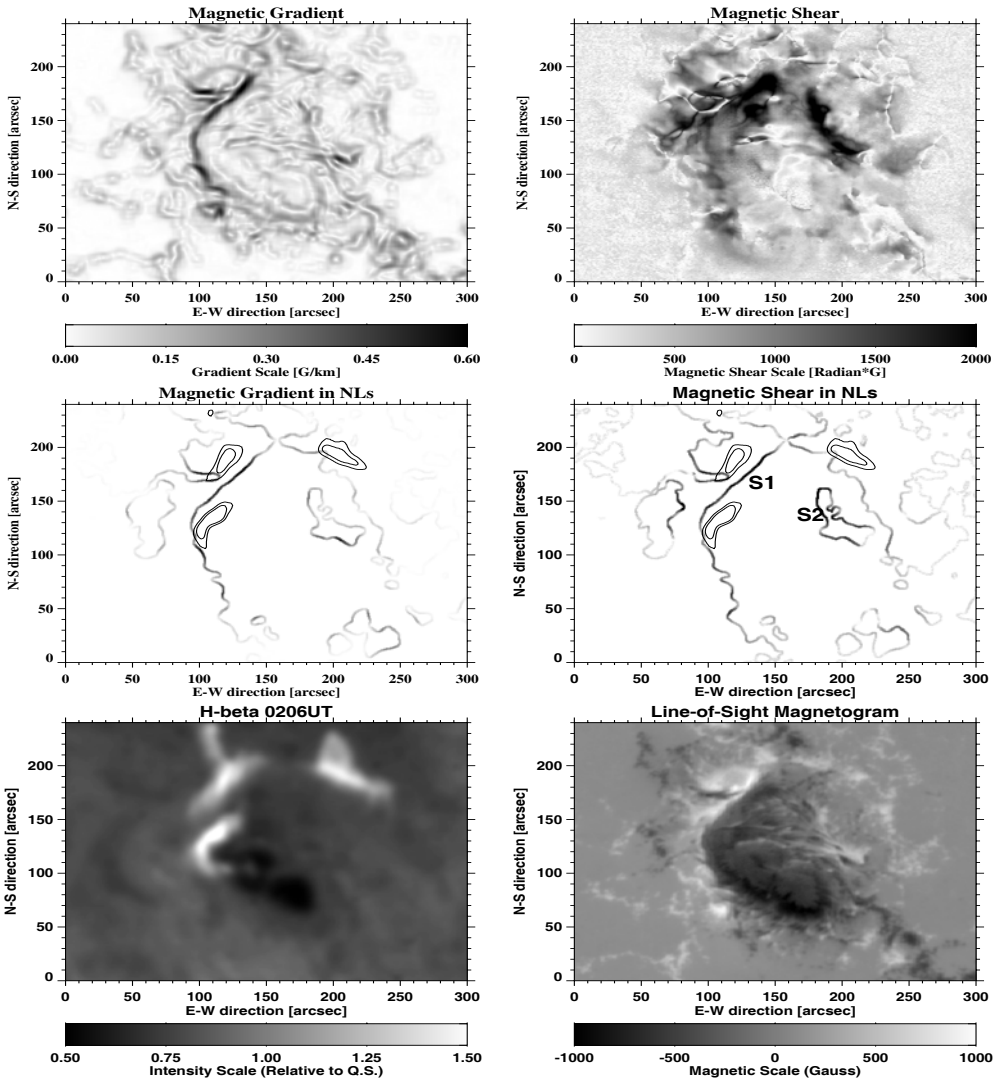

Fig. 4 Top left: magnetic gradient map of 1991 June 9; Top right: magnetic shear map; Middle left: magnetic gradient in neutral lines with flare contours; Middle right: magnetic shear in neutral lines with flare contours; Bottom left: Hβ image to indicate the flare emissions; Bottom right: line-of-sight magnetogram.

general, all the events have scatter plots similar to Figure 2: the shear and gradient are correlated, the flare neutral line seems to have both higher gradient and shear. The measurement errors discussed in Section 2 are at least one order of magnitude smaller than the physical quantities presented here.

In Table 2, we also present three parameters describing the relationship between the shear and gradient. If we consider all the neutral lines in the active regions, the correlation coefficients are between 64% and 89%. However, if we only consider points along the flare neutral lines, then, the coefficients are between 87% and 96%. Thus, the correlation between shear and gradient is well established.

For our data analysis procedures and results presented in this paper, it is natural to raise the following concern: since we did not convert the data from the observed coordinate system to the heliographic coordinate system, the neutral lines computed by the line-of-sight component of the magnetic field are not the same as that calculated from the longitudinal fields measured in the heliographic system. Consequently, the

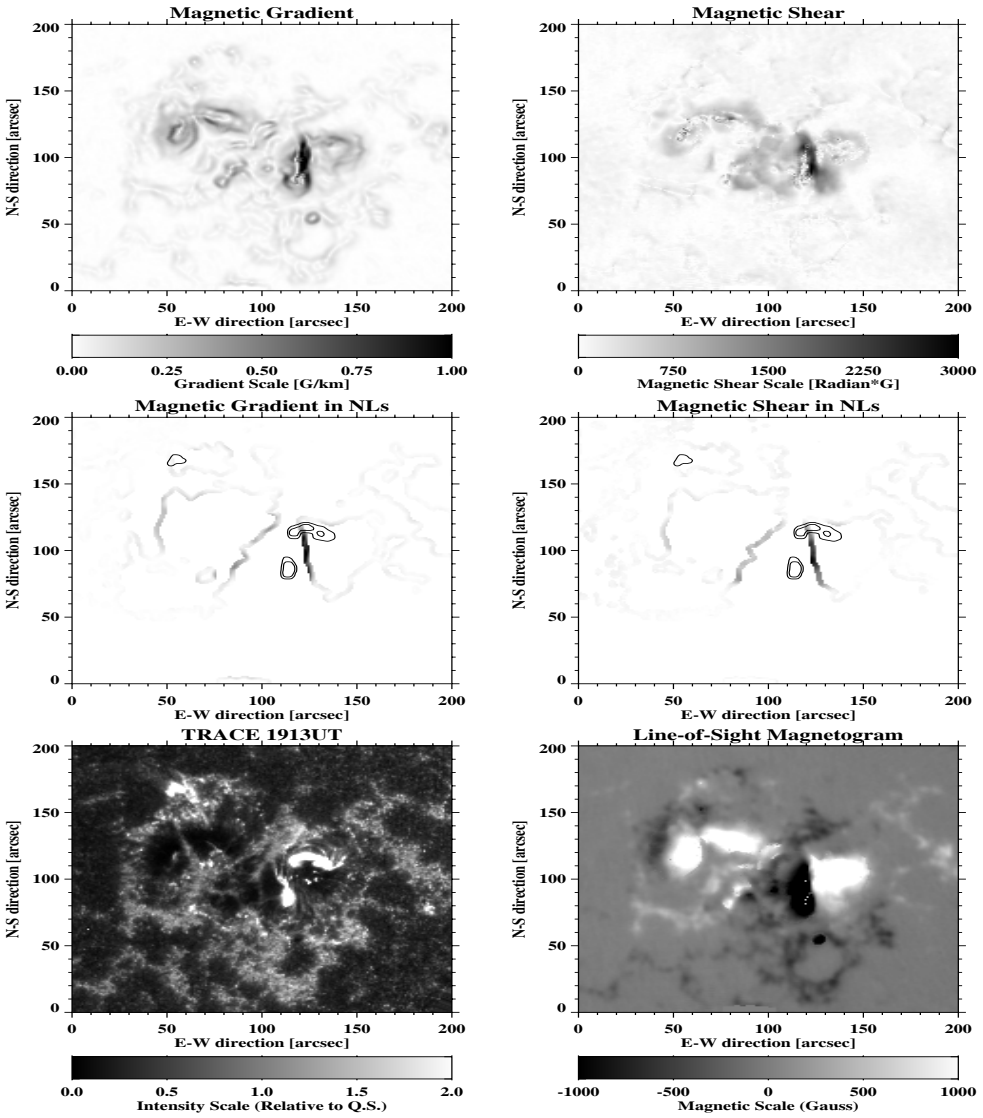

Fig. 5 Top left: magnetic gradient map of 2001 April 6; Top right: magnetic shear map; Middle left: magnetic gradient in neutral lines with flare contours; Middle right: magnetic shear in neutral lines with flare contours; Bottom left: TRACE 1600 Å image to indicate the flare emissions; Bottom right: line-of-sight magnetogram.

calculated gradient and shear angles from the observed transverse fields would have limitations due to this projection effect. Ideally, we should correct these effects. We did not do so for the following reasons:

(1) As we stated earlier, Li (2002) simulated the projection effects, and found that they would add about 10% to our uncertainty at the largest off-center position of the observed regions.
(2) We applied the coordinate conversion codes to the 2001 April 6 event, which had the largest angular position away from the disk center. Table 3 compares the results based on the corrected and uncorrected magnetograms. It is obvious that all the main conclusions in the present paper are still valid: maximum shear (or gradient) is located in the flare neutral line; mean shear (or gradient) along the flare neutral line is one order of magnitude larger than the mean value in the entire AR.

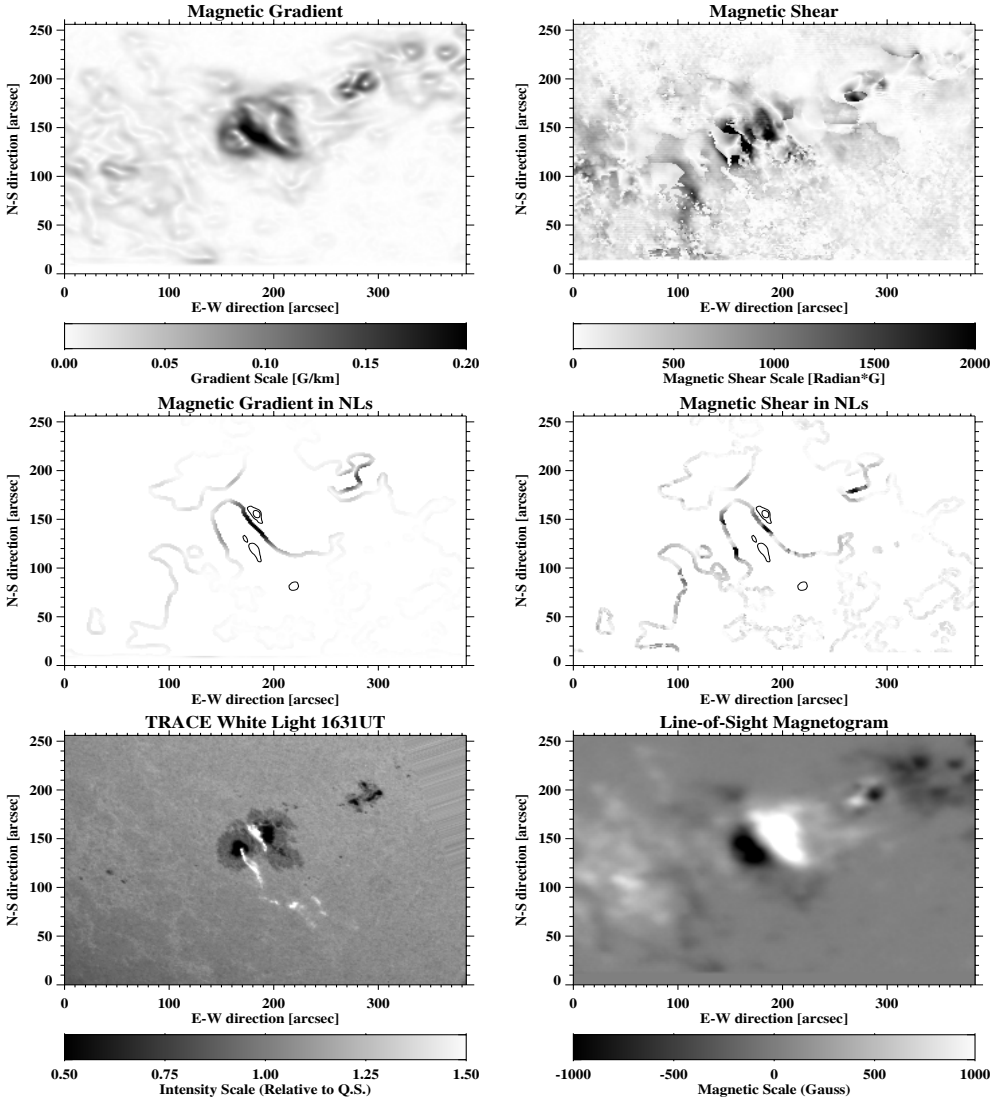

Fig. 6 Top left: magnetic gradient map of 2001 August 25; Top right: magnetic shear map; Middle left: magnetic gradient in neutral lines with flare contours; Middle right: magnetic shear in neutral lines with flare contours; Bottom left: TRACE WL image to indicate the flare emissions; Bottom right: line-of-sight magnetogram.

(3) We noted a drop in the correlation coefficient from about 90% to 80% in the relationship between the gradient and the shear. We believe that the projection correction added noise to the gradient maps. From Table 1 it is evident that the transverse fields' uncertainty is about an order of magnitude higher than that of the line-of-sight fields. After we mix the measured line-of-sight and transverse fields, the differential operation to calculate the gradient would increase the noise significantly. This error due to the random noise plus other errors, such as imperfect correction of the 180-degree uncertainty and calibration errors, will cause the results based on corrected magnetograms to suffer a larger amount of uncertainty. Therefore, we only selected events that are not too close to the solar limb and presented results based on the analysis of magnetograms without correction of the projection effect.

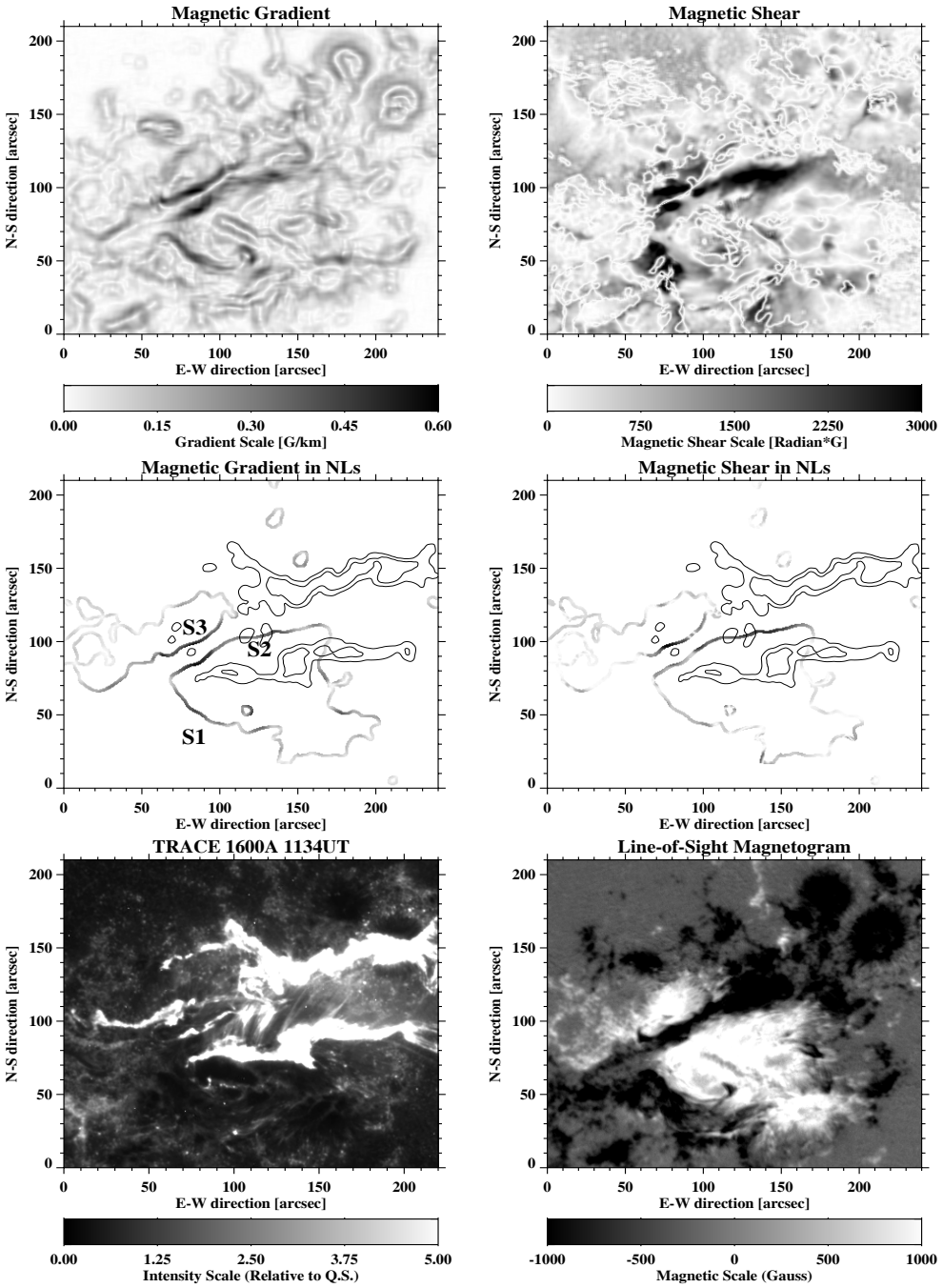

Fig. 7 Top left: magnetic gradient map of 2003 October 28; Top right: magnetic shear map; Middle left: magnetic gradient in neutral lines with flare contours; Middle right: magnetic shear in neutral lines with flare contours; Bottom left: TRACE 1600 Å image to indicate the flare emissions; Bottom right: line-of-sight magnetogram.

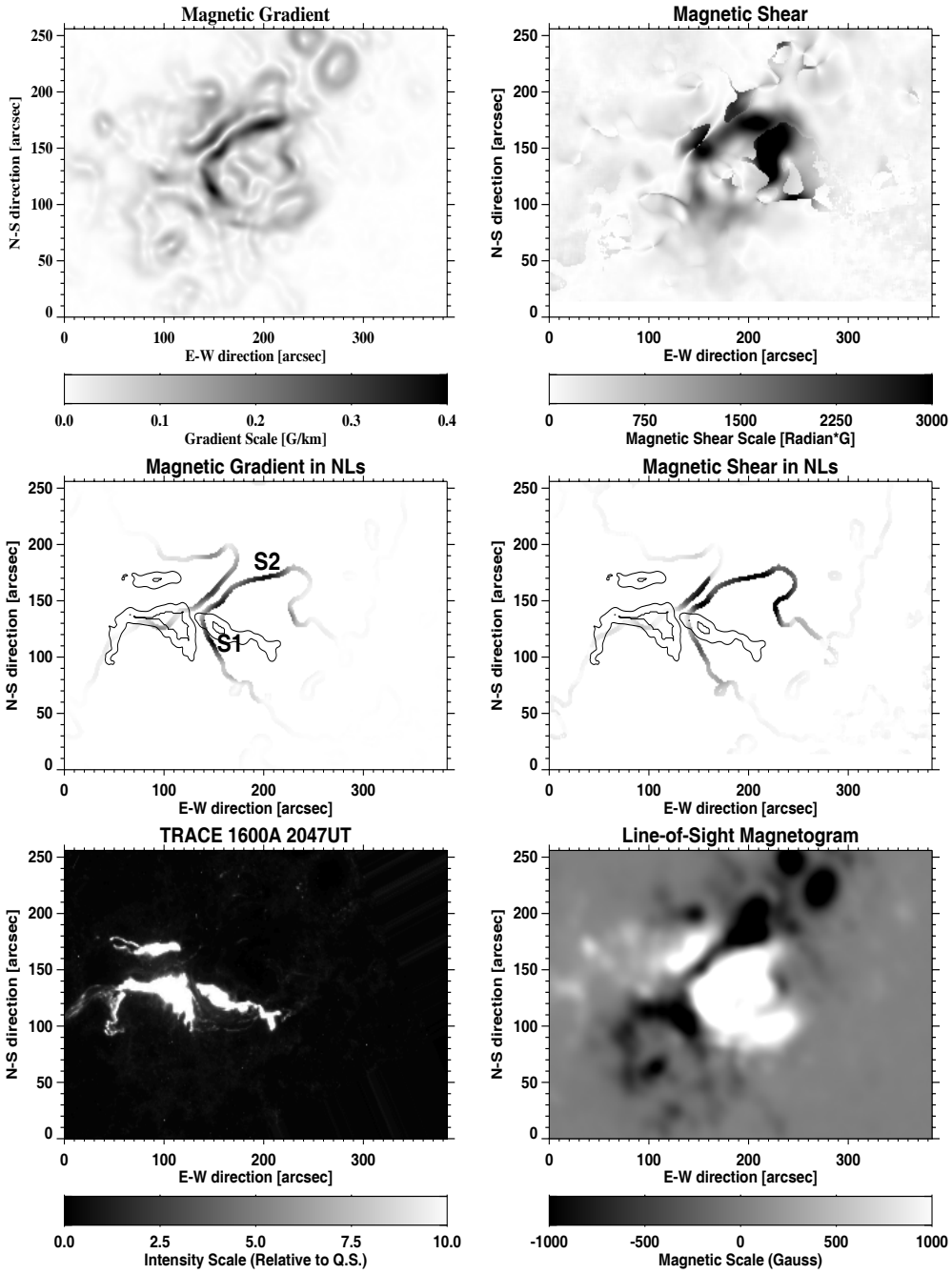

Fig. 8 Top left: magnetic gradient map of 2003 October 29; Top right: magnetic shear map; Middle left: magnetic gradient in neutral lines with flare contours; Middle right: magnetic shear in neutral lines with flare contours; Bottom left: TRACE 1600 Å image to indicate the flare emissions; Bottom right: line-of-sight magnetogram.

4 SUMMARY AND DISCUSSION

By analyzing vector magnetograms from four observatories for five well-known super-active regions, we found significant correlation between magnetic gradient and magnetic shear. Furthermore, we found that magnetic gradient might be even a better proxy to locate where a large flare occurs: all six flares occurred in the neutral line with the maximum gradient. If we use magnetic shear as the proxy, then the flaring neutral line of at least one (2001 August 25 event), and possibly two (2003 October 29 event), of the six events would be mis-identified. Please note that the weakness of using shear as a flare predictor might be caused by the limitation of ground based vector magnetograms and the difficulty in data analysis, such as the 180-degree ambiguity resolution and cross-talk among the Stokes components. Clearer conclusions will be obtained when high quality space data from Solar-B and SDO are available and data analysis methods are mature.

Magnetic gradient maps have been posted in the Active Region Monitor page daily (Gallagher, Moon & Wang 2002), they are being used as one of the parameters for solar flare prediction. The results presented in this study have provided evidence that magnetic gradient is important in real time activity monitoring and forecasting.

Acknowledgements We thank the referee for helpful comments that improved the paper. We are grateful to observing staff in BBSO, HSOS, MSO and MSFC for their support in obtaining the data. The work is supported by US NSF under Grants ATM-0548952 and ATM-0536921, NASA under Grant NAG5-13661, and the National Natural Science Foundation of China (NSFC, Grant 10228307).

References

Ai G., 1987, Pub. Beijing Astron. Obs., 9, 27
Deng Y., Wang J., Yan Y., Zhang J., 2001, Sol. Phys., 204, 11
Falconer D. A., 2001, JGR, 106, 25185
Falconer D. A., Moore R. L., Gary G. A., 2003, JGR, 108, SSH11
Fletcher L., Hudson H. S., 2001, Sol. Phys., 204, 69
Gallagher P. T., Moon Y. J., Wang H., 2002, Sol. Phys., 209, 171
Hagyard M. J., Smith J. B. Jr., Teuber D., West E. A., 1984, Sol. Phys., 91, 115
Kosovichev A. G., Zharkova V. V., 2001, ApJ, 550, L105
LaBonte B. J., Mickey D. L., Leka K. D., 1999, Sol. Phys., 189, 1
Li H., 2002, ChJAA, 2, 174
Liu Y., Zhang H., 2001, A&A, 372, 1019
Masuda S., Kosugi T., Hudson H. S., 2001, Sol. Phys., 204, 55
Michard R., 1971, IAU Symp., 43, 259
Mickey D. L., Canfield R. C., Labonte B. J. et al., 1996, Sol. Phys., 168, 229
Moon Y.-J., Wang Haimin, Spirock Thomas J. et al., 2003, Sol. Phys., 217, 79
Prasad C. B., 2000, Astrophysics and Space Science, 274, 463
Severny A. B., 1960, Izv. Krymsk. Astrofiz. Obs., 22, 12
Spirock T. J., 2005, Ph.D. Thesis, New Jersey Institute of Technology
Tanaka K., 1991, Sol. Phys., 136, 133
Tang F., 1983, Sol. Phys., 89, 43
Wang H., Varsik J., Zirin H. et al., 1992, Sol. Phys., 142, 11
Wang H., Ewell M. W., Zirin H., Ai G., 1994, ApJ, 424, 436
Wang H., Liu C., Zhang H., Deng Y., 2005, ApJ, 627, 1031
Yan Y., Deng Y. et al., 2001, ApJ, 551, L115
Zhang H., 2001, ApJ, 557, L71
Zhang H., Labonte B., Li J. et al., 2002, ApJ, 213, 87
Zirin H., Liggett M. A., 1987, Sol. Phys., 113, 267